Journal of Water Process Engineering 45 (2022) 102499

Contents lists available at ScienceDirect

Journal of Water Process Engineering

journal homepage: www.elsevier.com/locate/jwpe

Ceramic-supported graphene oxide membrane bioreactor for the anaerobic decolorization of azo dyes

Mohammad Shaiful Alam Amin [a,b], Frank Stüber [a], Jaume Giralt [a], Agustí Fortuny [c], Azael Fabregat [a], Josep Font [a,*]

[a] Universitat Rovira i Virgili, Departament d'Enginyeria Química, Avinguda Països Catalans, 43007 Tarragona, Catalunya, Spain
[b] Shahjalal University of Science and Technology, Department of Chemical Engineering and Polymer Science, Sylhet 3114, Bangladesh
[c] Universitat Politècnica de Catalunya, Departament d'Enginyeria Química, EUPVG, Av. Víctor Balaguer, s/n, 08800 Vilanova i la Geltrú, Catalunya, Spain

ARTICLE INFO

Keywords:
Graphene oxide
Membrane
Azo dye
Anaerobic decolorization

ABSTRACT

A continuous compact membrane bioreactor consisted of ceramic-supported graphene oxide membrane (CSGoM) was implemented for the first time for anaerobic biodecolorization of monoazo Acid Orange 7 (AO7), diazo Reactive Black 5 (RB5), and triazo Direct Blue 71 (DB71) solutions, showing excellent decolorization potential. The membrane was prepared by vacuum filtration of various graphene oxide solutions using a UF ceramic flat element. The decolorization efficiency of the CSGoM bioreactor, made from 1 $mg{\cdot}mL^{-1}$ of GO solution (B-CSGoM-1), was investigated for several structurally distinct azo dyes, initial feed concentrations, and permeate fluxes. Maximum color removal was achieved under low feed concentration (50 $mg{\cdot}L^{-1}$) and permeate flux (0.05 $L{\cdot}m^{-2}{\cdot}h^{-1}$), reaching 99% for AO7, 96% RB5, and 92% for DB71. At this low permeate flux, the biodecolorization was stable for all azo dye solutions irrespective of the feed concentration. In a subsequent experiment under higher feed concentration and permeate flux (100 $mg{\cdot}L^{-1}$ and 0.10 $L{\cdot}m^{-2}{\cdot}h^{-1}$), the decolorization slightly fell to 93%, 85%, and 81% for monoazo, diazo, and triazo solutions, respectively. The existence of anaerobic bacteria (*Geobacter* and *Pseudomonas guangdongensis*) in the B-CSGoM-1 biofilm confirms that they could perform efficient biodegradation of azo dye molecules in association with the graphene oxide membrane.

1. Introduction

Global water pollution occurred in all sources, including canals, lakes, rivers, oceans, and underground reservoirs. It usually happened when unwanted substances, from either humankind or environment, mix with water. Industrial effluents are the primary source of contaminant substances for water pollution. For instance, every year, 0.28 million tons of textile dyes are discharged in the aquatic environment as industrial waste [1]. About half of the textile dyes belong to the azo dye group, which is also extensively used in leather, medical, food, and personal care products [2,3]. The disposal of this untreated dyestuff poses a severe threat to the aquatic ecosystem as well as biodiversity [4]. It changes the natural appearance of the water becoming a dark, opaque, and colored liquid hindering the photosynthesis process due to the deficient transmission of sunlight in such water [5]. The dye effluents and their decomposed products are mostly detrimental, even at a very low concentration. This contaminated water, if used for drinking, household, or agricultural purposes, may cause toxicity, mutagenicity, and carcinogenicity on the human body [6]. Therefore, efficient wastewater treatment is highly required to maintain and control water pollution in this situation.

Several methods for treating dye-containing wastewater have been investigated, including physicochemical (adsorption, coagulation-flocculation, filtration, ion exchange), biological, photocatalysis by UV irradiation, advanced oxidation processes, and combined process [7,8]. Still, these treatment processes have faced some disadvantages, including addition of enormous amounts of chemicals, installation and operating costs, space requirements, secondary treatments, and poor process efficiency [9,10]. On the other hand, membrane-based separation processes have attracted tremendous attention in the wastewater treatment over the few decades due to its easy operation, low operating cost and energy consumption, small carbon footprint, and environmental suitability [11–13]. Besides, other eco-friendly, efficient dye removal processes are those based on biological mechanisms. Among the various biological methods, anaerobic treatments are very simple, less expensive azo dye removal processes [14]. This also produces less

* Corresponding author.
E-mail address: jose.font@urv.cat (J. Font).

https://doi.org/10.1016/j.jwpe.2021.102499
Received 14 September 2021; Received in revised form 2 December 2021; Accepted 3 December 2021
Available online 22 December 2021
2214-7144/© 2021 The Authors. Published by Elsevier Ltd. This is an open access article under the CC BY-NC-ND license (http://creativecommons.org/licenses/by-nc-nd/4.0/).

potentially dangerous substances, which eliminates the need to treat subsequently the biodegradable byproducts [7,15]. However, no single process for removing azo dyes from textile effluent is efficiently and economically viable yet [16]. Therefore, the advantages of both anaerobic pathway and membrane separation process can be coupled in a single compact reactor as a successful technique for the intensified biodecolorization of azo dye. The key for implementing effectively this alternative is the selection of membrane precursors that can successfully be coupled with the anaerobic process.

In this sense, nowadays, graphene oxide (GO) is considered a prospective precursor for the synthesis of membranes because of its unique two-dimensional structure that consisted of the functional polar oxidized zone and pristine graphite zone [17]. The water molecules accumulate inside the interlayers of the oxidized region, and the other zone increases the liquid permeation [18]. Besides, the nanoporous GO membrane imparts surface functionality, electrical conductivity, and mechanical stability, making it possible to produce a low-cost membrane for a large-scale operation such as wastewater treatment and molecular separation [19]. Pure GO (single or multilayer graphene) and GO composite (GO surface-modified, stacked graphene, graphene mixed-matrix) membrane are reported to be fabricated by filtration-assisted, casting, spin coating, and layer by layer assembly method [20]. Vacuum-assisted filtration is most commonly used to obtain either free-standing or supported GO membranes of all preparation techniques. In recent years, GO and GO-composite membranes have demonstrated the ability to retain azo dyes [17,21]. Still, it is under consideration to further improve the GO membrane durability, longevity, and water permeability without losing decolorization performance. So, it is important to obtain a compact treatment process with stable, robust, and high azo dye removal potential.

A nano-sized ceramic-supported carbon membrane (CSCM) was synthesized in our earlier work [22]. This form of the membrane was capable of decolorizing structurally different azo dyes. However, the effectiveness of the decolorization was limited at higher permeate flux and feed concentration, while it is an essential matter to attain the maximum decolorization performance for practical application. Taking this into account, this work is aimed at finding a robust and durable compact anaerobic membrane bioreactor for a better biodecolorization rate. The novelty of this study lies on the application of conductive graphene oxide membrane in combination with the anaerobic biofilm process for the successful removal of azo dye from dye-containing wastewater. It is worth that anaerobic bacteria such as *Geobacter* and *Pseudomonas* can perform extracellular electron transfer in an aqueous solution. As a result of the use of microorganisms and GO membrane, both the bacteria and the GO layer provide faster and more efficient electron transfer the dye azo bond (—N═N—) breaking, thus enhancing the decolorization performance under anaerobic conditions. Additionally, the nano-sized ceramic-supported graphene oxide membrane (CSGoM) acts as biofilm support and pollutant immobilizer to improve the azo dye removal rate. The optimum concentration of the GO solution for the preparation of CSGoM and its decolorization performance by anaerobic biodegradation were examined. Ceramic-supported graphene oxide membrane bioreactor (B-CSGoM) was first implemented for the monoazo Acid Orange 7 (AO7) decolorization process. Afterward, variations of critical parameters for B-CSGoM performance, for example, azo dye with different structures, molecular weight and functional groups, initial feed concentration, and permeate flux, were explored to enhance and optimize the bioreduction of azo dyes. Finally, the biofilm was examined to identify microbial species involved in this anaerobic process in order to understand and, subsequently, improve the biodecolorization by means of CSGoM.

2. Experimental

2.1. Fabrication of ceramic-supported GO Membrane

Vacuum-assisted deposition of the synthesized graphene oxide layer over the ceramic support (ZrO_2-TiO_2 ultrafiltration flat membrane; diameter: 47 mm; thickness: 2.5 mm; molecular weight cut-off: 50 kg·mol^{-1}; TAMI Industries, France) was used to prepare the CSGoM membrane. Firstly, a modified Hummer method [23] was employed to obtain the graphene oxide powder. A homogeneous mixture of 2.5 g of graphite powder (<20 μm, Sigma-Aldrich, ref. 282863) and 2 g of $NaNO_3$ (Honeywell Fluka™, ref. 15603430) was made in 70 mL of H_2SO_4 (Honeywell Fluka™ 95–98%, ref. 32051) solution. The mixture was then placed in an ice bath and mixed with 10 g of $KMnO_4$ (PanReac AppliChem, ref. 141527), and followed by stirring overnight at 50 °C. Thereafter, 10 g of $KMnO_4$ and 70 mL of Milli-Q water (Millipore Milli-Q system, Molsheim, France) were added and stirred for 24 h. The mixture was transferred into a beaker containing 400 mL of ice water, and 3 mL of H_2O_2 (Acros Organics, ref. 411,880,025) were added and kept stirred at room temperature. The graphite oxide solution was purified by a 500 mL solution of 0.5 wt% H_2O_2 and 3 wt% H_2SO_4. The graphite oxide pellet was centrifuged at 3000 rpm and the supernatant discarded. After repeating it five times, the solid was exfoliated in water in a sonication bath for 2 h to obtain graphene oxide. The GO pellets were dried for 48 h at 60 °C and then grounded using mortar and pestle to obtain the GO powder.

The schematic diagram of the synthesis of CSGoM is illustrated in Fig. 1. The process begins with preparing different concentrations of homogeneous GO solution (mg·mL^{-1}) by dissolving the desired amount of previously synthesized GO powder in deionized water, which was sonicated by 45 min in an ultrasonic bath. Then, 5 mL of GO solution was poured over the ceramic support placed inside the filtration cell (INSIDE DisRAM holder, TAMI Industries, France). After 15 min of vacuum filtration, a controllable graphene oxide layer was formed on the ceramic support surface. The coating was settled by first drying at 80 °C for 24 h and then at 100 °C for 72 h. Following the above procedure, a total of four GO membranes were prepared using a variety of precursor concentrations; these were denoted as CSGoM-0.5, CSGoM-1, CSGoM-2, and CSGoM-4, respectively, for the membrane synthesized with 0.5, 1, 2, and 4 mg·mL^{-1} of exfoliated GO solutions.

2.2. Experimental set-up for anaerobic biodegradation

Fig. 2 shows a scheme of the lab-scale B-CSGoM system used in this study. The compact bioreactor was made of a filtration cell that held the CSGoM membrane with 5 mL of retentate chamber. AO7 (ACROS Organics, ref. 416561000), diazo Reactive Black 5 (RB5) (Sigma-Aldrich, ref. 306452), and triazo Direct Blue 71 (DB71) (Sigma-Aldrich, ref. 212407) were selected as model compounds to generate the artificial wastewater. As co-substrate, Sodium Acetate (SA) (Sigma-Aldrich, ref. 110,191) was used as a carbon source and electron donor for microorganisms and azo reduction. The dye and SA were dissolved in Milli-Q water at a 1:3 mass ratio to make the synthetic feed solution. After that, 1 mL of each basic medium (BM), used as a source of microorganism nutrients, was added to the feed solution. There were six basal media; BM 1 contained 0.155 mg·L^{-1} $MnSO_4·H_2O$, 0.285 mg·L^{-1} $CuSO_4·5H_2O$, 0.46 mg·L^{-1} $ZnSO_4·7\ H_2O$, 0.26 mg·L^{-1} $CoCl_2·6H_2O$ and 0.285 mg·L^{-1} $(NH_4)_6Mo_7O_{24}$; BM 2 contained 21.75 mg·L^{-1} K_2HPO_4, 33.40 mg·L^{-1} $Na_2HPO_4·2H_2O$, 8.50 mg·L^{-1} KH_2PO_4; BM 3 was 29.06 mg·L^{-1} $FeCl_3·6H_2O$ solution; BM 4 was 13.48 mg·L^{-1} $CaCl_2$ solution; BM 5 was 15.2 mg·L^{-1} $MgSO_4·7H_2O$ solution; and BM 6 was 190.90 mg·L^{-1} NH_4Cl solution. All the chemicals used in this BM were analytical grade chemicals (Sigma-Aldrich), and the solutions of these chemicals were made by dissolution in Milli-Q water.

The feed solution was kept at 1 °C to prevent microbial growth in the feed stream that ensured a stable sodium acetate concentration. The

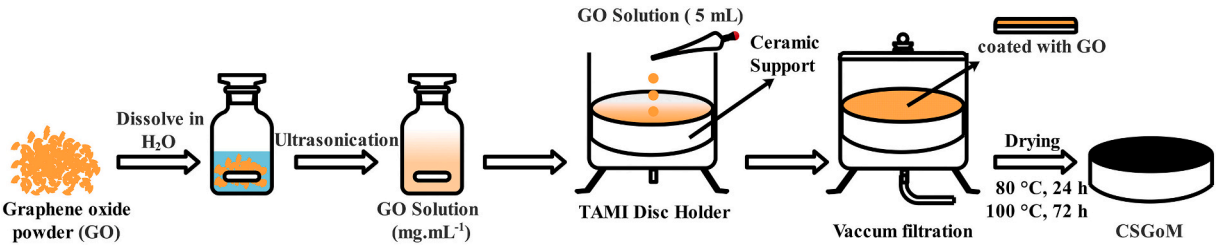

Fig. 1. Fabrication process of the ceramic-supported GO Membrane (CSGoM).

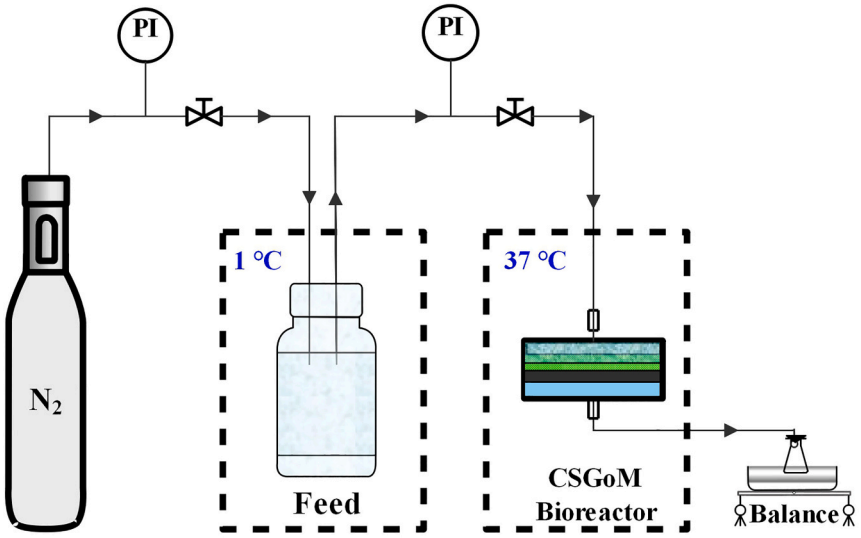

Fig. 2. CSGoM bioreactor experimental set-up.

reactor was sealed tightly after 5 mL of secondary anaerobic sludge (municipal WWTP Reus, Spain) was placed over the CSGoM. Continuous sparging of nitrogen through the feed solution (Purity > 99.99%, Linde) helped to maintain the negative redox potential, needed to favor dye decolorization rate [24]; this resulted in the obtained anaerobic conditions throughout the system. Moreover, nitrogen pressure fixed the operation of TMP, thus controlling the permeate flux. The compact bioreactor was run under dead-end filtration mode at a temperature of 37 ± 1 °C to boost the efficiency of microbial strains that were capable of decoloring azo dyes [25,26].

2.3. Ceramic-supported graphene oxide membrane characterization

The morphology, thickness, and elemental composition of graphene oxide membranes were characterized by the Field Emission Scanning Electron Microscope with Focused Ion Beam (FESEM-FIB, Scios 2 Dual Beam, Thermo Scientific, USA). Atomic Force Microscopy (AFM, Molecular Imaging Pico Plus 2500, Bid Service, USA) was used to examine the membrane surface and conductivity.

Raman scattering measurements to characterize the carbon product were carried out at room temperature with a Renishaw inVia Raman Confocal Microscope System w/Leica DM 2500 M at 633 nm. Furthermore, to confirm the phase purity and crystallinity of the CSGoM membrane, a Siemens D5000 diffractometer, Bragg-Brentano parafocusing geometry, and vertical θ-θ goniometer under the CuK_α wavelength of 1.54056 Å at 40 kV and 30 mA, was used for X-ray Diffraction (XRD). The data was obtained using a sample rotation (0.05° angular step at 3 s per step) and analyzed with the aid of diffrac-plus software.

The filtration performance of CSGoM was inspected using Eqs. (1) and (2) as straightforward method to determine the flux and hydraulic resistance.

$$J = \frac{V}{t}\frac{1}{A} \tag{1}$$

$$H_R = \frac{\Delta P}{\mu}\frac{1}{J} \tag{2}$$

where J is the permeate flux (L·m^{-2}·h^{-1}), V the volume of permeate (L) collected in a given time, t the filtration time (h), A the membrane area (m^2), H_R is the resistance (m^{-1}), ΔP is the transmembrane pressure (bar), and μ is the viscosity (Pa·s) of the permeate corrected to experimental temperature.

Dye removal was evaluated by measuring the dye concentration using a UV/VIS4000n Spectrophotometer (DINKO Instruments, Spain) at the corresponding maximum absorbance wavelength at 484 nm for AO7, 597 nm for RB5, and 585 nm for DB71. The decolorization percentage (D) was calculated using Eq. (3).

$$D\,(\%) = \frac{A_o - A}{A_o} \times 100 \tag{3}$$

where A_o and A are the absorbance of feed and treated samples for each biodegradation test, respectively.

2.4. Microbial analysis

The microbial diversity of the biofilm evolved during the anaerobic bioreduction of dye was examined using DNA isolation kits (Norgen Biotek Corporation, ref. 64000). In this extraction technique, the biosamples were collected from the membrane surface and its DNA extracted [27]; 500 ng of extracted DNA were used for library preparation to apply DNA Illumina sequencing employing Illumina DNA Prep kit (Illumina, Inc.). All libraries were evaluated with the TapeStation

High Sensitivity DNA kit (Agilent Technologies) and quantified with Qubit (Invitrogen Corporation). The filtered reads were matched to unique clade-specific marker genes using MetaPhlAn 3 to determine the taxonomic profile. Relative abundances and alpha diversity measures (Shannon and chao1 indexes) were calculated using MetaPhlAn's relative proportions.

3. Result and discussion

3.1. Morphological structure of CSGoM

X-ray diffraction of the CSGoM-1 obtained by vacuum-assisted method is presented in Fig. 3. The GO crystal plane (0 0 1) is clearly visible at $2\theta = 11.5^{\circ}$ with the interlayer spacing of 0.76 nm that is larger than graphite atomic spacing, 0.33 nm [28]. This suggests that the oxygen functional group attached to the edge of each layer raises the spacing between the layers, which aids GO exfoliation in the aqueous medium [29]. There are no graphitic contaminants in the CSGoM-1, which is confirmed by the lack of peaks at $2\theta = 26^{\circ}$ [30]. The peaks at $2\theta = 30$, 35, 50 and 59° are due to the presence of tetragonal ZrO_2 [31], whereas the peaks at $2\theta = 28$, 43, 54 and 69° owns to rutile form of TiO_2 [32] in the ceramic support.

Raman spectra shown in Fig. 4 can provide additional evidence for the presence of GO in the CSGoM-1. High intensity peaks in the Raman spectra of CSGoM-1 indicate the expected conjugated and carbon-carbon double bonds of graphene. In general, the D peak is caused by sp^3 carbon atoms with a disordered or defective carbon structure, while the G peak is originated from the vibration of the aromatic structure of sp^2 hybrid carbon atoms. It also reflects the same characteristics as XRD, whereas the tetragonal ZrO_2 is observed at 262 cm^{-1} (E_g) [33] and for rutile TiO_2 peaks at 448 cm^{-1} (E_g) and 611 cm^{-1} (A_{1g}) [34]. The typical D and G bands for the CSGoM-1 are found at 1351 cm^{-1} and 1605 cm^{-1}, respectively. The quotient I_D/I_G, the D and G band's intensity ratio, is a common way to express the defect degree of materials. It is found to be 1.02 for CSGoM-1, which is consistent with reported values in the literature [35]. This ratio suggests that the GO membrane is relatively stable and resistant to environment conditions. Furthermore, the absence of a 2D band at 2700 cm^{-1} indicates that all the graphite layers were essentially oxidized during the oxide formation step [36].

The morphology of both CS and CSGoM-1 were examined by FESEM. Fig. 5(a–b) demonstrates that both ceramic support and ceramic-supported graphene oxide membranes are typical porous surfaces

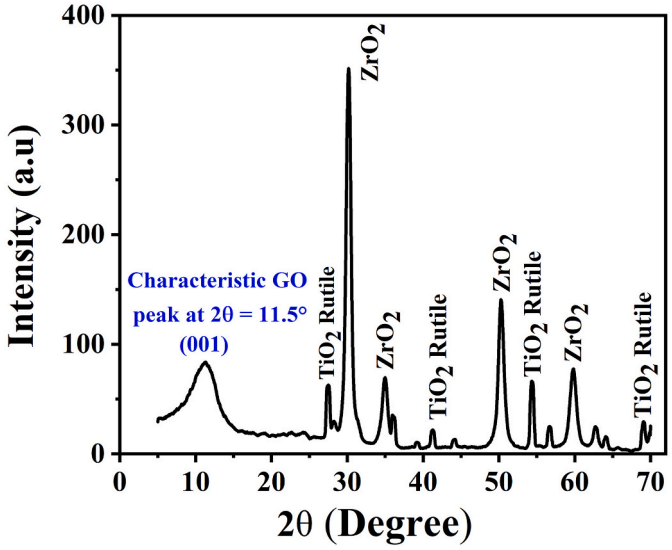

Fig. 3. XRD diffractogram of ceramic-supported graphene oxide membrane.

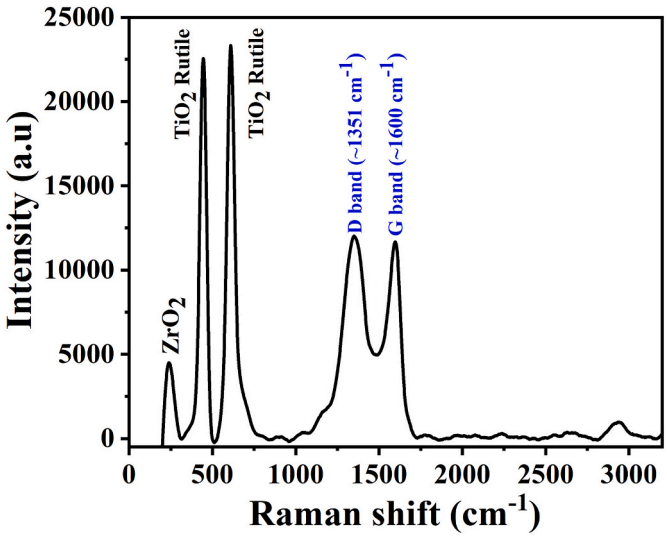

Fig. 4. Raman spectra of ceramic-supported graphene oxide membrane.

[22,37]. Part of the of the graphene oxide deposited on the ceramic support appears as an aggregate or was broken down into smaller particles that penetrated into the ceramic support to form a GO-ZrO_2 composite [23]. It seems that, once the pores were shrinking or blocked, the homogeneous GO layer was formed, over a first zone of the composite GO-ZrO_2 and then over the original ZrO_2 section. Probably, interaction on the membrane surface is mainly due to the attraction between ZrO_2 oxygens and either or both hydroxyl and carboxylic groups of graphene oxide [38,39]. As expected, the GO layer deposited reduced the pore size of the virgin CS surface. In addition to the visual inspection of the FESEM images, ImageJ software was used to analyze the surface pores of CS and CSGoM-1. Compared to the CS, it is found that the pore size of the CSGoM-1 is significantly lowered, where more than 80% of the pores being around 25 nm, in the range of transition from ultra to nanofiltration.

The cross-sectional images of both CS and CSGoM-1 (Fig. 5(c–d)) revealed a clear disparity between the support and the membrane. The bottom part in both cases is the titanium oxide layer. There are then two more layers of zirconium oxide above the titanium oxide layer: the smaller active porous layer and the intermediate porous layer.

However, another layer is clearly visible in the CSGoM-1, which corresponds to the synthesized graphene oxide membrane. This configuration is in line with that found by Octávia et al. [40], who demonstrated the fabrication of a uniform GO-Zirconia composite membrane. The 1.55 μm thick GO layer is firmly adhered to the ceramic support, indicating the success of CSGoM-1 preparation using the vacuum-assisted method.

Table 1 lists the GO content and elementary composition of CSGoM synthesized with various concentrations of GO solution. As expected, the GO content (0.8 to 3.9 mg) of the top layer of CSGoM increases in proportion to the initial solution concentration of membrane precursors. The FESEM-EDX analysis of the GO membrane provided more detailed information about this layer composition. As expected, the results show that CS is made of ZrO_2 and TiO_2, although the content of zirconia is higher than titania as the analysis rather falls upon the upper layer of the virgin layer, described as a selective zirconia band. In turn, the CSGoM have a carbon-rich layer on top (13.7 to 66.8 wt% of carbon) together with ZrO_2 and TiO_2. The amount of carbon content is greater when increasing the concentration of exfoliated GO solution during coating and, subsequently, the relative content of ZrO_2 and TiO_2 is decreased. Obviously, the data is in accordance with the fact that the incident beam energy (5 keV) for all measurements penetrated a given depth through the CSGoM surface. Thus, the thicker GO layer on the membrane surface

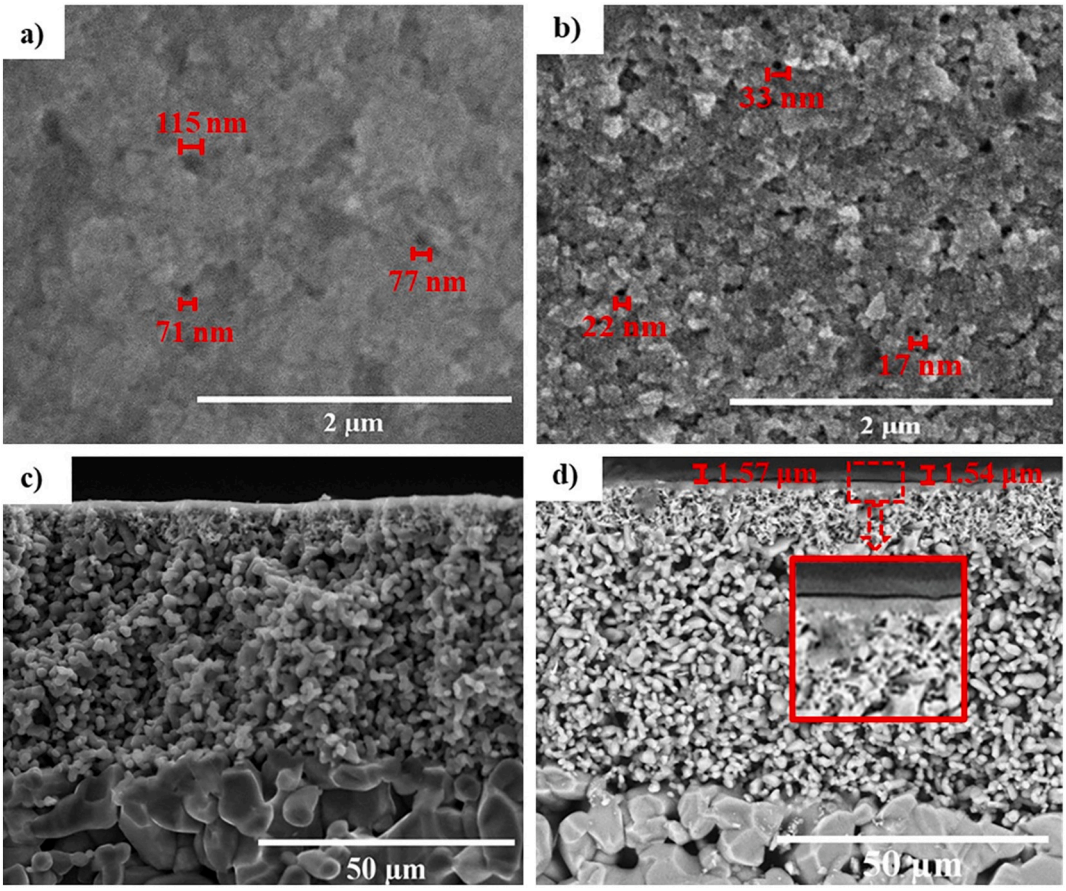

Fig. 5. FESEM micrographs on the surface of a) CS and b) CSGoM-1, and the cross section of c) CS and d) CSGoM-1 (deposited GO amounts: 2.6 mg).

Table 1
Surface analysis of the CS and CSGoM.

	GO content	C	O	Ti	Zr
	(mg)	(wt%)			
CS	n.d.	n.d.	44.0	22.2	33.8
CSGoM-0.5 (0.5 mg·mL^{-1})	0.8	13.7	42.2	17.0	27.1
CSGoM-1 (1 mg·mL^{-1})	2.6	49.4	37.0	3.1	10.5
CSGoM-2 (2 mg·mL^{-1})	3.3	61.3	35.9	n.d.	2.8
CSGoM-4 (4 mg·mL^{-1})	3.9	66.8	33.1	n.d.	0.1

allows passing a shorter distance, and therefore the analysis was able to quantify fewer elements deeper inside the membrane composite. Furthermore, as the concentration of the precursor solution rises, more GO particles begin to penetrate the GO-ZrO_2 composite layer, which means deposited deep inside the ceramic support. As a result, the precursor concentration increases from 2 to 4 mg·mL^{-1} had almost no significant changes in the carbon content measured on the membrane surface.

The multilayer 3D topography, height, and current profile of CSGoM-1 were investigated by using AFM (at a random area of 500 × 500 nm^2) and CSAFM (current sensing atomic force microscopy); the data is shown in Fig. 6(a–b). The mean roughness and root mean square (RMS) roughness analysis of the membrane surface yielded 7.5 and 9.4 nm, respectively. According to a rough estimate based on AFM imaging with SPIP™ software, most of the pores in CSGoM-1 were in the 17–33 nm range, which compares well with estimates made by FESEM.

The CSAFM images also provide the current distribution profile of the CSGoM-1 membrane (Fig. 6b). The results demonstrate the local conductance on graphene oxide surfaces, which should enhance the rate

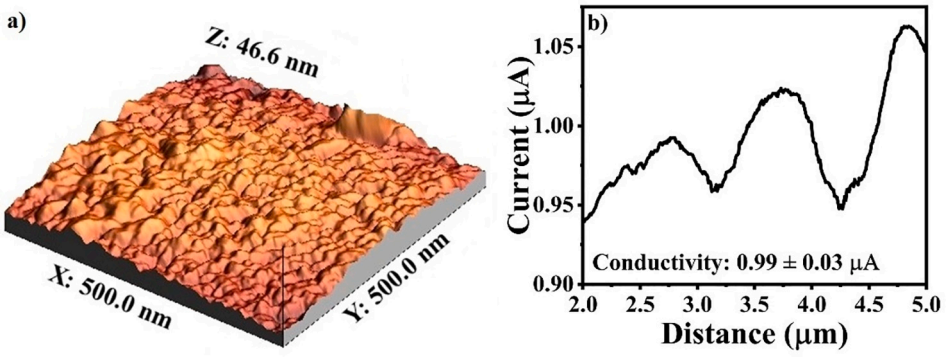

Fig. 6. AFM images of CSGoM-1 a) 3D Topography b) current distribution.

of biodegradation through the electron shuttle mechanism [41].

3.2. Impact of the GO layer on flux resistance

A set of tests were conducted to investigate the effect of depositing different amounts of membrane precursor (produced by varying the concentration of GO solution) on filtration characteristics represented by membrane flux, and the derived parameters pure water permeability (PWP) and hydraulic resistance (H_R). As expected, the membrane without GO, CS, showed the highest flux, 62.3 $L{\cdot}m^{-2}{\cdot}h^{-1}$. The pure water flux of the ceramic support (ZrO_2-TiO_2 based ultrafiltration flat membrane) is mainly influenced by the membrane properties such as thickness, homogeneity, and porosity. Additional single or multilayer GO was formed over the ceramic support in CSGoM, resulting in an increment of hydraulic resistance. Moreover, the GO particles reduce the pore size of the ceramic support. Thus, a membrane without the GO always possessed the highest water flux. Similar results are shown in Fig. 7, where the flux decreased linearly with increasing GO thickness, which correlates with the increasing precursor concentration for CSGoM preparation (0.5, 1 and 2 $mg{\cdot}mL^{-1}$ GO). The lowest pure water flux (4.1 $L{\cdot}m^{-2}{\cdot}h^{-1}$) was observed for the membrane made of 2 $mg{\cdot}mL^{-1}$ of GO solution (CSGoM-2). In comparison to CS, the pure water flux for CSGoM-0.5, CSGoM-1, CSGoM-2 dropped 63%, 83%, and 93%, respectively. Giménez et al. [23] also found strong flux drops, 47% and 77%, for GO membranes prepared from 0.05 and 0.5 $mg{\cdot}mL^{-1}$ of GO over a 0.04 μm pore size ceramic support. The derived PWP follows these trends, so CS exhibits maximum permeance (77.8 $L{\cdot}m^{-2}{\cdot}h^{-1}{\cdot}bar^{-1}$) and it then decreases up to 5.1 $L{\cdot}m^{-2}{\cdot}h^{-1}{\cdot}bar^{-1}$ for CSGoM-2 (Fig. 7).

From the permeances given in Fig. 7, the total resistance of the CS and CSGoM were estimated, and the specific contribution of the GO layer was calculated considering the ceramic support resistance to be constant in the membranes containing GO. The hydraulic resistance of the ceramic support was estimated to be as $5.2 \pm 0.1 \cdot 10^{12}$ m^{-1}. It has been noted that GO load during preparation of graphene oxide membranes has a significant impact on permeate flux, thus in the hydraulic resistance. Since permeate flux and hydraulic resistance are interconnected functions, higher graphene oxide content membrane must result in more resistance. During fabrication, the ceramic support pores (GO-ZrO_2 region) were first entirely filled and then formed on top the GO multilayer. It was also observed that the thickness of the deposited GO layer grew as the GO concentration was increased, which in turn decreased the membrane flux [42,43] and increased the hydraulic resistance. Hence, the CSGoM resistances increased from $1.51 \pm 0.04 \cdot 10^{13}$ m^{-1} to $8.64 \pm 0.13 \cdot 10^{13}$ m^{-1} as the concentration of GO solution during coating increased from 0.5 to 2 $mg{\cdot}mL^{-1}$. Therefore, the CS gives less than one third of the total resistance in CSGoM. Further increase of GO concentration up to 4 $mg{\cdot}mL^{-1}$ in CSGoM-4 preparation made the membrane essentially impermeable due to the formation of a very thick, dense, and nonporous GO layer on the membrane surface that prevents water molecules from passing across [44,45].

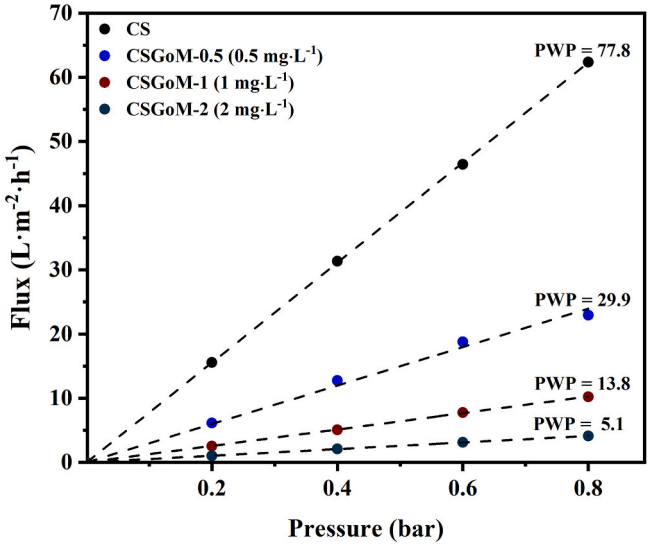

Fig. 7. Variation of pure water flux and pure water permeability of CS and CSGoM at 25 °C. (PWP in $L{\cdot}m^{-2}{\cdot}h^{-1}{\cdot}bar^{-1}$).

On the other hand, a low concentration of GO solution (<0.5 $mg{\cdot}mL^{-1}$) failed to form a uniform, stable GO-Ceramic membrane because of lack of carbon content and non-homogeneous layer formation on the membrane surface. Lou et al. [46] found that a membrane prepared from 0.05, 0.10, and 0.5 $mg{\cdot}mL^{-1}$ GO solution was not good enough for practical application. Moreover, in a membrane prepared with a high GO concentration (≥4 $mg{\cdot}mL^{-1}$), the GO layer can peel up easily after swelling and detached from the surface. Therefore, it is inferred that the CSGoM preparation technique must meet two critical requirements. GO load must be suitable to create a homogeneous and tightly bound GO layer and permeate flux should be at the desired level. In this study, it was found that the CSGoM-1, with an estimated 1.55 μm GO layer thickness showed a permeability of 13.8 $L{\cdot}m^{-2}{\cdot}h^{-1}{\cdot}bar^{-1}$. This was comparable to other attempts available in the literature such as a polyacrylonitrile nanofibrous mat supported (8.2 $L{\cdot}m^{-2}{\cdot}h^{-1}{\cdot}bar^{-1}$) and an electrospray nanofiltration (11.3 $L{\cdot}m^{-2}{\cdot}h^{-1}{\cdot}bar^{-1}$) GO membrane [47]. Even though the carbon wall or channel is hydrophobic in nature, the slip flow theory indicates that it can assist in transporting the liquid between the GO layers [42]. As per this principle, the water molecules first proceed to the hydrophilic edges and defects of the GO layer, which act as a gate for water flow. The liquids are usually deposited in those gates and then slip through the hydrophobic nanochannel. As a result, graphene oxide membrane displays acceptable permeate flux despite having a thicker layer. Based on these facts, 0.5 and 1 $mg{\cdot}mL^{-1}$ of GO solution appears to be the optimum concentration for forming the membranes properly, combining enough flux and robustness needed for the wastewater treatment process.

3.3. Role of the graphene oxide layer on anaerobic biodecolorization of azo dyes

The capability of the graphene oxide membrane for anaerobic azo dye decolorization was checked out, with and without the formation of biofilm. Four different reactor combinations were used: mixed microbial consortium on CS (B-CS), mixed microbial consortium on CSGoM (B-CSGoM), no microbial consortium on CS (R-CS), and no microbial consortium on CSGoM (R-CSGoM). In all cases, initially, 50 $mg{\cdot}L^{-1}$ feed solution of AO7 was used as it falls within the typical range (10 to 50 $mg{\cdot}L^{-1}$) of dye concentrations in real textile effluents [48]. In all the cases, a constant flux of 0.05 $L{\cdot}m^{-2}{\cdot}h^{-1}$ was maintained in a dead-end filtration mode. Furthermore, two graphene oxide membranes produced from 0.5 and 1 $mg{\cdot}mL^{-1}$ of GO solution (CSGoM-0.5 and CSGoM-1) were used to investigate the impact of graphene oxide content on the decolorization process. As above commented, the thickness of the GO layer on the membrane surface is easily adjusted by changing the precursor concentration. Since the membrane flux is dependent on the thickness of the deposited graphene oxide layer (resistance) of the CSGoM, transmembrane pressure from 0.5 to 2.0 bar was adjusted in the experiments to maintain a constant flow irrespective of the different membrane thicknesses. Fig. 8 includes the removal evolution for all the cases during a period of 10 days, since the start until a steady operation was reached. Overall, the results confirmed that the presence of the GO layer had a significant effect on the decolorization of AO7. The color removal attained was larger at the highest GO load (B-CSGoM-1 consisting of the membrane made of 1 $mg{\cdot}mL^{-1}$ of GO solution), giving a decolorization of 99%.

All the reactors apparently showed a good efficiency during the first 12 h as they decolorized more than 75% of the azo dye solution.

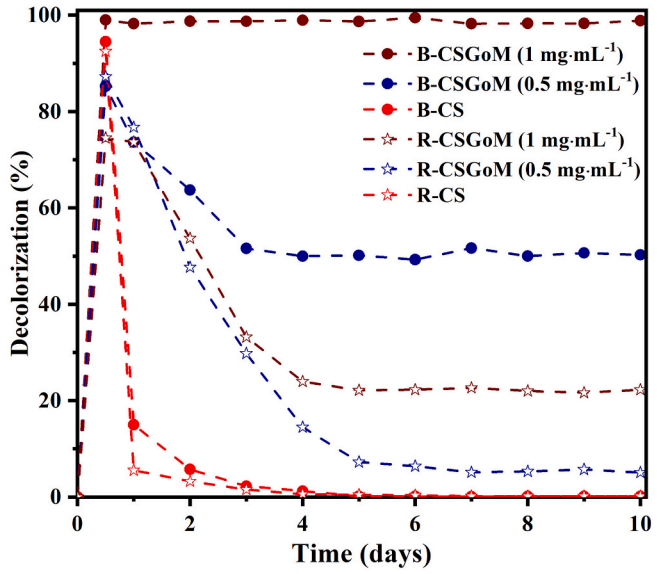

Fig. 8. Decolorization of AO7 in CS and CSGoM reactors; CS and CSGoM bioreactors; Flux = 0.05 $L{\cdot}m^{-2}{\cdot}h^{-1}$, AO7 concentration in feed solution = 50 $mg{\cdot}L^{-1}$ and T = 37 °C. (For interpretation of the references to color in this figure, the reader is referred to the web version of this article.)

Actually, this initial decolorization was basically due to the adsorption of the dye on the membrane surfaces, so it is not a true removal. Once the membrane became saturated, the color removal efficiency dropped suddenly, except for B-CSGoM-1, stabilizing rapidly around a mostly steady value. The B-CS and R-CS completely lost any decolorization ability after two days. In the case of R-CS, once saturated the membrane material, the only possible mechanism to remove dyes could be the membrane retention, which fails since the pore size of the support element (UF range) is too high in comparison to the dye dimensions (NF range). Although B-CS was operated with the mixed microbial consortium, the desired biodecolorization did not occur because of the probable absence of an active biofilm or even microorganisms on the ceramic support, which can probably be ascribed to the fact that the permeate flow washed out the bacteria before forming a biofilm because of their size relatively smaller than the support pores. After four days of operation, the decolorization rate stabilized at approximately 22% for R-CSGoM-1 and 10% after six days with R-CSGoM-0.5. In this case, the membranes are partially able to retain the dye due to the nano-sized pores of the CSGoM surface created after GO layer formation. Therefore, this limited capacity of dye removal can essentially be attributed to molecular sieving mechanism.

Only for B-CSGoMs (blue and brown circles in Fig. 8), there was a true biodegradation of the dye. The highest decolorization (98%) was observed for the B-CSGoM-1 prepared with a concentration of 1 $mg{\cdot}mL^{-1}$ of GO, whereas only 51% of color removal was observed using B-CSGoM-0.5 made from 0.5 $mg{\cdot}mL^{-1}$ GO. Only dye decomposition caused by the anaerobic action of the microorganisms can account for the high level of decolorization observed in this study. However, a great difference is observed between the performance of the B-CSGoM-1 and B-CSGoM-0.5, where the load of GO seems to favor the biodecomposition. To form an efficient biofilm or anaerobic membrane scaffold, microorganisms must be selectively attached to the graphene oxide surface. The essence of the microbial activity and the consistency of the GO layer have a direct impact on adhesion performance. Thus, the improved performance in B-CSGoMs was due to the concurrent occurrence of physical sieving and anaerobic biodegradation. As in previous studies using ceramic-supported carbon-based membrane bioreactors [22], the GO layer of B-CSGoM also played a triple role in the anaerobic decolorization of azo dyes since it performs as a pollutant immobilizer, support for the biofilm, and electron transporter. Graphene-oxide membranes are more conductive than Matrimid-based carbon membranes [22], thus contributing to a faster electron shuttle mediator mechanism. Moreover, the surface of the nanoporous graphene oxide membrane improves the microbial metabolism and retains the degradation products, which globally enhances the decolorization performance [49].

Compared with previous studies (the upflow packed-bed reactor filled with biological activated carbon) with a similar objective [50], the B-CSGoM-1 was also stabilized in a shorter retention time to achieve the almost complete (99%) decolorization of AO7. On the other hand, our configuration shows better performance if compared to other attempts based on GO. Shital et al. [51] assessed AO7 removal by adsorption with reduced graphene oxide (RGO), combined RGO-Photolysis, RGO-Oxidation with H_2O_2, and RGO-Oxidation with photo radiation process, and found 10% removal by RGO alone and a maximum of 80% by combined RGO-Oxidation with UV-radiation.

Since GO plays a critical role in this process, it was expected that its load in the GO layer impact someway on the dye removal. For instance, in an oxidation process, Lee et al. [52] investigated GO load and discovered that the increase of the load improved the dye removal efficiency. As previously noted, FESEM-EDX measurements (Table 1) confirmed the increase of the GO concentration in the precursor solution from 0.5 to 1 $mg{\cdot}mL^{-1}$ improves the GO content of CSGoM from 0.8 to 2.6 mg. This latter higher load creates a membrane with smaller pore size responsible of dye adsorption and biofilm immobilization, therefore, both enhanced [53]. Moreover, the carbon-rich CSGoM enhances the redox mediator role due to the greater availability of sites with redox properties, which also contributes to improve the biodegradation performance. Fig. 8 corroborates this trend, as raise of carbon content from 13.7% to 49.4% on CSGoM-1 almost doubled the decolorization (from 51 to 98%). Further application of a CSGoM-2 and CSGoM-4, as commented above, gave a less or non-permeable membrane, so the CSGoM-1 was taken as the most favorable balance between flux and decolorization.

3.4. *Effect of flux and feed concentration on azo dye decolorization*

The effect of feed concentration and permeate flux on the decolorization process of B-CSGoM-1 was evaluated by varying AO7 concentrations (50, 75, and 100 $mg{\cdot}L^{-1}$) and permeate fluxes (0.05, 0.075, and 0.10 $L{\cdot}m^{-2}{\cdot}h^{-1}$). All experiments were conducted for 30 days continuous operation, with a flow of 0.05 $L{\cdot}m^{-2}{\cdot}h^{-1}$ within the first 10 days, 0.075 $L{\cdot}m^{-2}{\cdot}h^{-1}$ for the second 10 days, and finally at 0.10 $L{\cdot}m^{-2}{\cdot}h^{-1}$ until the end. The transmembrane pressure (TMP) was adjusted when needed to keep a constant permeate flux. Though slight, accumulated membrane fouling during the process would lower the permeate flux if not corrected. Fig. 9 depicts the change in AO7 decolorization for the three feed concentrations tested during the three periods of different permeate flux. As can be seen, irrespective of the conditions, the decolorization reached over 90% although the expected trends for feed concentration and permeate flux were observed. B-CSGoM-1 with a feed concentration of 50 $mg{\cdot}L^{-1}$ and a permeate flux of 0.05 $L{\cdot}m^{-2}{\cdot}h^{-1}$ achieved the maximum AO7 removal, 99%. At a higher permeate flux (0.10 $L{\cdot}m^{-2}{\cdot}h^{-1}$), the decolorization slightly decreased to 97%, 95%, and 93%, at the AO7 feed solution concentrations of 50, 75, and 100 $mg{\cdot}L^{-1}$ respectively. Along with Fig. 9, Table 2 illustrates the amount of dye removed and the percentage of decolorization during the B-CSGoM-1 process. It is worth noting that when the feed concentration and permeate flux increase, decolorization usually reduces but the amount of decolorized dye is progressively growing. In this experiment, a maximum equivalent consumption of 9.3 $mg{\cdot}m^{-2}{\cdot}h^{-1}$ was obtained for 100 $mg{\cdot}L^{-1}$ AO7 at a 0.10 $L{\cdot}m^{-2}{\cdot}h^{-1}$ flux.

Color removal was thoroughly stable at the low flux-region, with no significant differences observed for the three different feed concentrations. The low permeate flow allowed the dye molecules to interact with

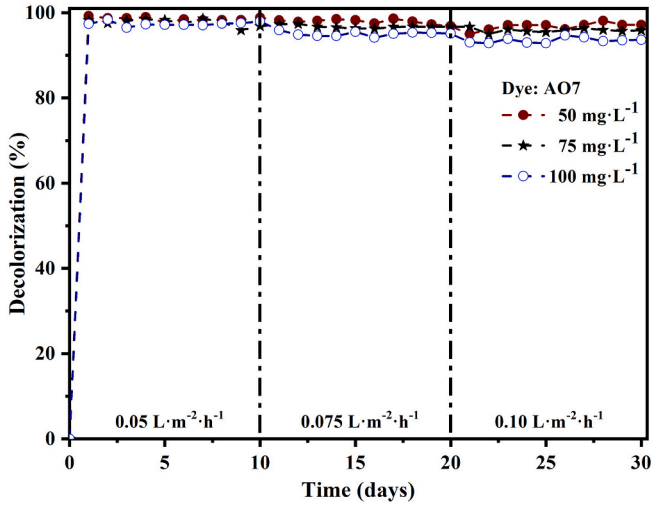

Fig. 9. Influence of feed concentration and permeate flux on anaerobic decolorization of AO7 using B-CSGoM-1.

Table 2
Summary of the decolorization and dye removal in B-CSGoM-1 tests.

	Decolorization (%)			Dye removal rate (mg·m⁻²·h⁻¹)		
Flux (L·m⁻²·h⁻¹) / Concentration (mg·L⁻¹)	0.05	0.075	0.10	0.05	0.075	0.10
50	99	98	97	2.5	3.7	4.7
75	98	97	95	3.7	5.4	7.2
100	97	95	93	4.9	7.1	9.3

bacteria enough time to reach large biodegradation [54]. After 30 days of operation, even increasing permeate flux, the B-CSGoM-1 gave around 99% of azo dye decolorization for the 50 mg·L^{-1} feed solution. Increasing the flux, even the falling decolorization percentage, the absolute amount of AO7 removal by the B-CSGoM-1 increased from 2.5 to 4.7 mg·m^{-2}·h^{-1}. These decolorization and dye removal findings concluded that the amount of biomass was sufficient to assure almost complete biodegradation of the dye. Anyway, even when the AO7 feed concentration and permeate flux doubled, the microorganisms were able to attain high levels of decolorization. Thus, the decolorization for 75 and 100 mg·L^{-1} feed solution at 0.075 and 0.10 L·m^{-2}·h^{-1} flux was only reduced to 98–95% and 97–93%, respectively. Simultaneously, the Total Organic Carbon (TOC) and Chemical Oxygen Demand (COD) of each dye solution were reduced by more than 85% and 95%, respectively, in all conditions. The effluent properties achieved by B-CSGOM-1 were highly suitable for environmental emissions (details are given in Table A). Besides, these conditions furnish more absolute dye removal, which reach 7.1 and 9.3 mg·m^{-2}·h^{-1} for 75 and 100 mg·L^{-1} feed solutions, respectively. The results were much better than those obtained using conventional discontinuous biological systems at several AO7 concentrations [50,55,56]. In a similar reactor configuration and operations conditions using carbon-based membranes instead of GO [22], the decolorization attained was 58%, 45%, and 36% for 50, 75, and 100 mg·L^{-1} of AO7 solutions, respectively, while over 93% removal was achieved using the present B-CSGoM-1 in the ranges tested. This suggests that the GO plays a dominant role during the dye biodegradation, being much more efficient than carbon-based membrane made using Matrimid 5218 as a precursor [22]. Probably the potential of GO as a redox mediator enhanced the transfer of electrons to the azo bond of the dye molecule, leading to easier cleavage of the azo bond [57]. However, regardless of the color removal, this compact bioreactor unit is more compatible with higher feed concentration and permeate flux to remove the amount of azo dye as the microorganisms of the B-CSGoM-1 is highly capable of coping with the growing dye loads. Consequently, it might be more productive to operate the B-CSGoM-1 at a greater permeate flux.

3.5. Comparative decolorization of azo dyes

A comparative biodecolorization of three structurally different azo dyes (mono azo AO7, diazo RB5, and triazo DB71) were investigated in the anaerobic B-CSGoM-1s under various permeate fluxes and feed concentrations. The extent of decolorization of azo dye solutions varied depending on the number of azo bonds present in the dye structure. Fig. 10(a–c) illustrates this fact. In general, for the three azo dyes, the decolorization declined as feed concentration and permeate fluxes increased. As expected, for all experimental conditions, mono azo AO7 dye reported the highest color removal (99–93%), which was significantly higher than for diazo (96–85%) and triazo (92–81%) dyes. Franciscon et al. [58] previously demonstrated that the monoazo dye removal was faster and more efficient than diazo and triazo using a sequential microaerophilic-aerobic treatment with *Klebsiella* sp. strain VN-3. Anyway, the absolute quantity of dye removal for all azo dyes as well progresses with increasing feed concentration or permeate flux, although it reduces when raising the number of azo bonds and AO7 hence exhibits the highest dye removal of 9.3 mg·m^{-2}·h^{-1} while DB71 the lowest 8.1 mg·m^{-2}·h^{-1}.

It must be considered that the contact time (directly related to the permeate flux) can affect the removal capacity, which is also varied depending on dye properties and microorganism behavior against each

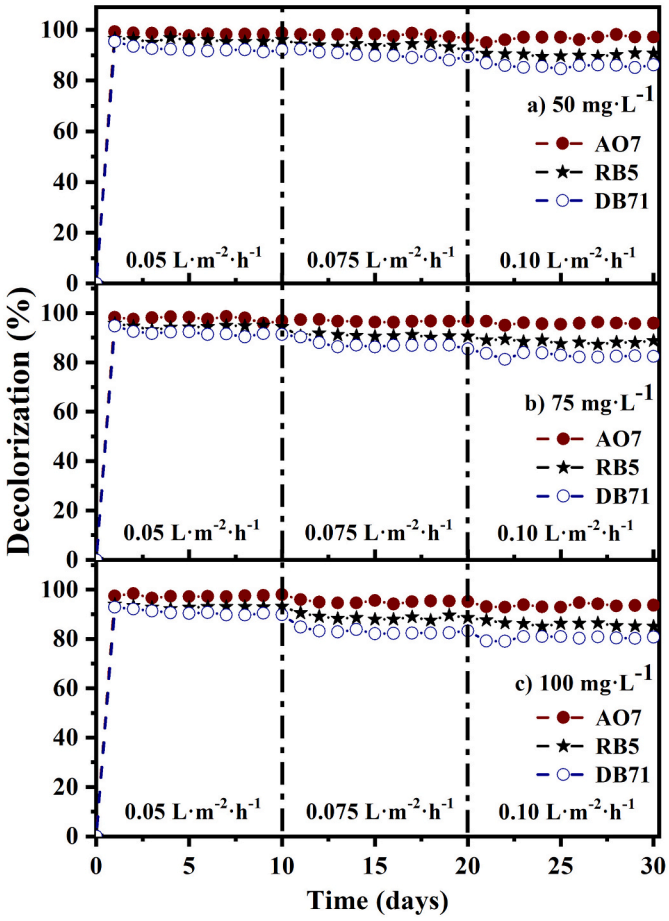

Fig. 10. Anaerobic decolorization of AO7, RB5, and DB71 dyes at various concentrations and fluxes; a) 50 mg·L^{-1}, b) 75 mg·L^{-1} and c) 100 mg·L^{-1} dye solution at 37 °C.

specific dye [59]. In B-CSGoM-1, as when increasing feed concentration, a higher permeate flux adds additional dye load with more chromophores and auxochromes content in the decolorization process. Additionally, the high flux minimizes biomass retention time within the bioreactor, thereby declining microbial biodecolorization [60,61]. As a result, under high feed concentration (100 mg·L^{-1}), changing permeate flux from 0.05 to 0.075 L·m^{-2}·h^{-1} and finally to 0.10 L·m^{-2}·h^{-1}, the decolorization reduced to 93% for AO7, 85% for RB5, and 81% for DB71. The corresponding dye removal for AO7, RB5, and DB71 was calculated to be 9.3, 8.5, and 8.07 mg·m^{-2}·h^{-1}, respectively.

Under identical operating conditions, the structural properties and nature of the azo dyes, for example, meta, ortho, and para position of the electron-withdrawing groups (—NO_2, —C≡N, —SO_3H, —SO_2NH_2) to azo bond, presence of electron-releasing groups (—OH, —R, —NH_2) and other functional groups (—CH_3, O—CH_3), the number of azo bonds and high molecular weight of the dye molecules have been reported to cause variations in decolorization rate [62–64]. Increase of both permeate flux and feed dye concentration, brought more reactive groups into the anaerobic bioreactor. It has been reported that an excess amount of —SO_3H groups in the azo dye structure readily reduced microbial growth [65]. In addition, a rise of toxicity in the degradation process led to inadequate biomass to dye ratio and spoiled the active sites of the biofilm. Consequently, microbial biomass yield at higher feed concentration probably remains lower due to excess dye toxicity to microorganisms. Compatible trends can be seen in Fig. 10(a–c), in which the percentage of decolorization of AO7 declines as the initial feed concentration or permeate flux increases. Anyway, it has been proved that the bioreactor configuration here introduced successfully decolorized the various azo dyes tested, in line with results reported elsewhere [22,66].

3.6. Microbial community analysis

Since the active biofilm evolved from conventional secondary sludge taken from a municipal WWTP after an acclimation period, it is interesting to elucidate which type of microorganism remained prevalent for the dye biodegradation. Therefore, FESEM analysis was applied to measure the presence of microorganisms in the B-CSGoM biofilm after the DB71 biodegradation. Fig. 11(a–b) displays the surface and cross-sectional view of the biofilm formed over the GO layer. On the biofilm surface, significant quantities of microorganisms with an average size of 1.51 μm were detected. Cross-section analysis revealed a biofilm thickness of about 1.83 μm over the GO membrane (Fig. 11c).

The biofilm specimen of distinct B-CSGoM-1 bioreactors was used to extract the DNA of bacteria. Three DNA samples were collected from the CSGoM-1 bioreactors operated with 50, 75, and 100 mg·L^{-1} of DB71 solutions and were then compared with the original anaerobic sludge (inoculum). DNA Illumina sequencing was used to examine the microbial populations of bacteria, archaea, viruses, and single-celled eukaryotes in these four samples. The sequencing run produced 32.8 million reads that reduce to 30.6 million reads after quality filtering. Although raw anaerobic sludge contained both bacteria and archaea, no archaea were found after bioreactor operation. Fig. 12 depicts the schematic bar diagram and comparison of bacterial phyla for the four samples.

According to species richness, chao1 indexes show that anaerobic sludge (15.24) was the most diverse, and B-CSGoM-1 with 50 mg·L^{-1} DB71 (7.54) was less. Overall, among the 53 bacterial taxonomic units (OTUs), the species *Pseudomonas guangdongensis* was the most prevalent in all samples, while *Geobacter sulfurreducens* was abundant in all biofilms but not in the initial anaerobic sludge. In all cases, bacterial growth solely depended on the concentration of feed solution. For example, the presence of a significant number of *Geobacter sulfurreducens* (35%) was observed in the biofilm that treated 100 mg·L^{-1} DB71 solution, and the lowest (7%) was found for 50 mg·L^{-1} of DB71 solution. Similarly, presence of *Pseudomonas guangdongensis* in biofilm was enhanced increasing inflow dye concentration, but the highest was still in the original anaerobic sludge. The results revealed that activities of both *Geobacter sulfurreducens* and *Pseudomonas guangdongensis* were increased with increasing dye concentration.

Several studies have proven the role of *Geobacter sulfurreducens* in the anaerobic biodegradation of azo dye solution [67,68]. Moreover, the extracellular electron transfer capability of *Geobacter sulfurreducens* and *Geobacter soli* might enable them to play an important role during the biodecolorization process [69]. In addition, *Geobacter anodireducens*, which were present in B-CSGoM-1, can exchange more electrons and more rapidly than *Geobacter sulfurreducens* and *Geobacter soli* [70]. Higher content of these bacteria in B-CSGoM-1 operated with 50 mg·L^{-1} of DB71 could contribute to get a more stable and better decolorization performance (as shown in Fig. 10a). Nevertheless, other bacterial species such as *Stenotrophomonas acidaminiphila* [71], *Pseudomonas guangdongensis* [72], *Cupriavidus metallidurans* [73] were known as a potential decolorizing organism. All they were significantly present in B-CSGoM biofilm and probably took part in the decolorization.

4. Conclusions

To the best of our knowledge, this is the first time that a dead-end membrane filtration element with a ceramic-supported graphene oxide layer has been used for anaerobic azo dye decolorization. Different concentrations of GO solution were examined to investigate their formation of CSGoM and subsequent performance over the anaerobic biodecolorization process. Due to the suitable membrane permeability, resistance, and maximum decolorization during the azo dye removal process, CSGoM-1 made from 1 mg·mL^{-1} GO solution was identified as the optimal for this integrated compact bioreactor that provides a novel, robust, and effective color removal process.

The conductive surface of the GO membrane enhances faster electron transfer in B-CSGoM if compared to other carbon-based processes reported. In all operating conditions, the dye removal performance for monoazo AO7 was stable and higher than for RB5 and DB71. High decolorization rates of structurally distinct azo dyes (99% for AO7, 96%

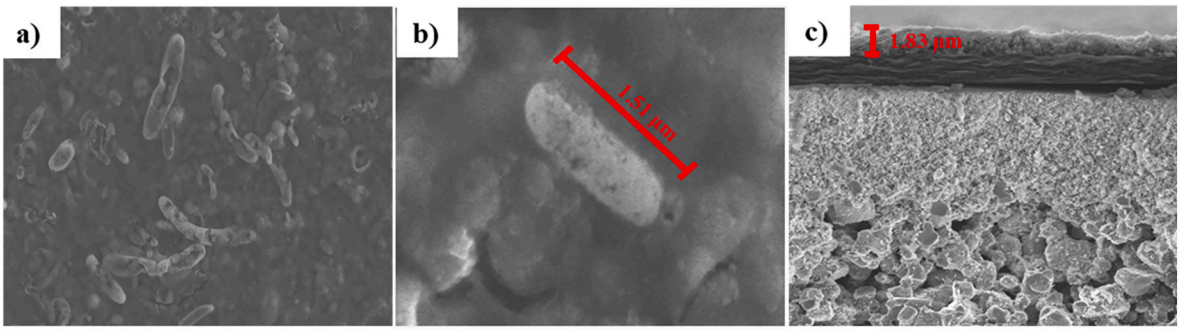

Fig. 11. Micrograph of FESEM images of biofilm sample after biodecolorization of azo dyes. a) Biofilm surface b) size of the microorganism c) biofilm thickness.

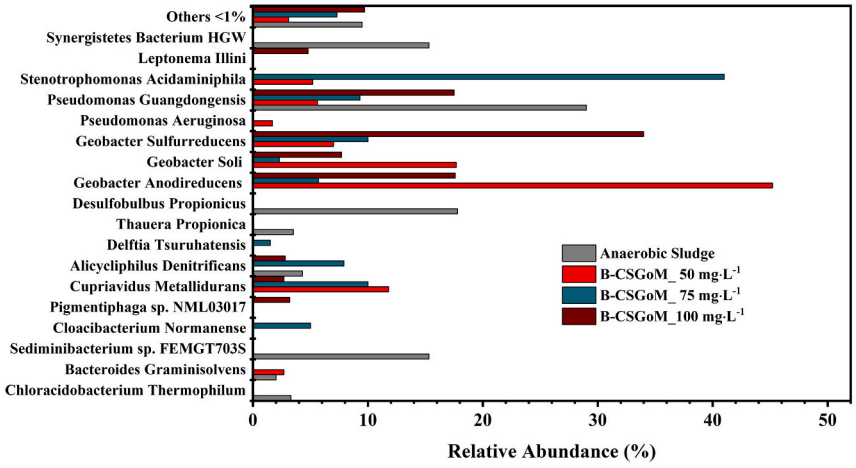

Fig. 12. Schematic bar diagram of bacterial phyla in the B-CSGoM-1; (▭) Anaerobic sludge, B-CSGoM-1 of (▭) 50 mg·L^{-1}, (▭) 75 mg·L^{-1} and (▭) 100 mg·L^{-1}.

for RB5, and 92% for DB71) were achieved at the lowest permeate flux (0.05 L·m^{-2}·h^{-1}) and feed concentration (50 mg·L^{-1}).

The microbial community found in the B-CSGoM-1 mainly contained anaerobic *Geobacter* (*Soli*, *Anodireducens*, *Sulfurreducens*) and *Pseudomonas guangdongensis*; all are recognized to be able to decolorize azo dyes in anaerobic conditions.

Declaration of competing interest

The authors declare that they have no known competing financial interests or personal relationships that could have appeared to influence the work reported in this paper.

Acknowledgements

This project has been supported by the European Union's Horizon 2020 research and innovation programme under the Marie Skłodowska-Curie grant agreement No. 713679 and by the Universitat Rovira i Virgili (URV), contract 2017MFP-COFUND-18. This article was possible thanks to the grant RTI2018-096467-B-I00 funded by MCIN/AEI/10.13039/501100011033 and "ERDF A way of making Europe". The authors research group is recognized by the Comissionat per a Universitats i Recerca, DIUE de la Generalitat de Catalunya (2017 SGR 396), and supported by the Universitat Rovira i Virgili (2019PFR-URV-33). We would like to thank Dr. Constantí for her contribution to the bacterial community characterization.

Appendix A. The properties of feed and permeate quality

The typical properties of the dye-containing feed solution and treated effluent quality are listed in Table A.

Table A
Water quality of the feed and treated effluent.

Dye	Concentration	TOC[a,b]		COD[a,b]	
		Feed	Effluent	Feed	Effluent
AO7	50	86.8	6.4	310	10
	75	96.9	7.9	340	8
	100	102.4	7.8	410	9
RB5	50	56.3	12.2	220	7
	75	70.2	10.3	259	8
	100	88.6	14.3	319	7
DB71	50	53.42	8.6	208	12
	75	83.3	13.4	296	13
	100	110.5	5.7	382	13

[a] Unit of the concentration, TOC and COD are in (mg·mL^{-1}).
[b] The TOC and COD measurements were analyzed by Lovibond testing kit vials Vario 420761 and Vario 2420710 respectively.

References

[1] X.-C. Jin, et al., Decolorization of a dye industry effluent by aspergillus fumigatus XC6, Appl. Microbiol. Biotechnol. 74 (1) (2007) 239–243.
[2] S. Garcia-Segura, E. Brillas, Combustion of textile monoazo, diazo and triazo dyes by solar photoelectro-Fenton: decolorization, kinetics and degradation routes, Appl. Catal. B Environ. 181 (2016) 681–691.
[3] Y. Chen, et al., Biodegradation and detoxification of direct black G textile dye by a newly isolated thermophilic microflora, Bioresour. Technol. 250 (2018) 650–657.
[4] A.B. dos Santos, et al., Review paper on current technologies for decolourisation of textile wastewaters: perspectives for anaerobic biotechnology, Bioresour. Technol. 98 (12) (2007) 2369–2385.
[5] M.F. Elshahawy, et al., Fabrication of TiO2 reduced graphene oxide based nanocomposites for effective of photocatalytic decolorization of dye effluent, J. Inorg. Organomet. Polym. Mater. 30 (7) (2020) 2720–2735.
[6] B. Lellis, et al., Effects of textile dyes on health and the environment and bioremediation potential of living organisms, Biotechnol. Res. Innov. 3 (2) (2019) 275–290.
[7] V. Prigione, et al., Fungal waste-biomasses as potential low-cost biosorbents for decolorization of textile wastewaters, Water 4 (4) (2012).

[8] M.J. Uddin, et al., Preparation of nanostructured TiO2-based photocatalyst by controlling the calcining temperature and pH, Int. Nano Lett. 2 (1) (2012) 19.
[9] F.I. Hai, et al., Hybrid treatment systems for dye wastewater, Crit. Rev. Environ. Sci. Technol. 37 (4) (2007) 315–377.
[10] M.A. Islam, et al., Optimal design of an activated sludge plant: theoretical analysis, Appl. Water Sci. 3 (2) (2013) 375–386.
[11] M.A. Shannon, et al., Science and technology for water purification in the coming decades, Nature 452 (7185) (2008) 301–310.
[12] K. Goh, et al., All-carbon nanoarchitectures as high-performance separation membranes with superior stability, Adv. Funct. Mater. 25 (47) (2015) 7348–7359.
[13] D.L. Gin, R.D. Noble, Designing the next generation of chemical separation membranes, Science 332 (6030) (2011) 674.
[14] Y. García-Martínez, et al., Fast aqueous biodegradation of highly-volatile organic compounds in a novel anaerobic reaction setup, Environments 5 (2018) 115.
[15] D.V. Savant, et al., Anaerobic degradation of adsorbable organic halides (AOX) from pulp and paper industry wastewater, Bioresour. Technol. 97 (9) (2006) 1092–1104.
[16] F.P. van der Zee, S. Villaverde, Combined anaerobic–aerobic treatment of azo dyes—a short review of bioreactor studies, Water Res. 39 (8) (2005) 1425–1440.
[17] K.H. Thebo, et al., Highly stable graphene-oxide-based membranes with superior permeability, Nat. Commun. 9 (1) (2018) 1486.
[18] D.R. Dreyer, et al., The chemistry of graphene oxide, Chem. Soc. Rev. 39 (1) (2010) 228–240.
[19] J. Ma, et al., Recent developments of graphene oxide-based membranes: a review, Membranes 7 (3) (2017).
[20] N. Song, et al., A review of graphene-based separation membrane: materials, characteristics, preparation and applications, Desalination 437 (2018) 59–72.
[21] P. Zhang, et al., Cross-linking to prepare composite graphene oxide-framework membranes with high-flux for dyes and heavy metal ions removal, Chem. Eng. J. 322 (2017) 657–666.
[22] M.S.A. Amin, et al., Comparative anaerobic decolorization of azo dyes by carbon-based membrane bioreactor, Water 13 (8) (2021) 1060.
[23] A. Giménez-Pérez, et al., Synthesis of N-doped and non-doped partially oxidised graphene membranes supported over ceramic materials, J. Mater. Sci. 51 (18) (2016) 8346–8360.
[24] N.D. Lourenço, et al., Effect of some operational parameters on textile dye biodegradation in a sequential batch reactor, J. Biotechnol. 89 (2) (2001) 163–174.
[25] M.S. Khehra, et al., Decolorization of various azo dyes by bacterial consortium, Dyes Pigments 67 (1) (2005) 55–61.
[26] M. El Bouraie, W.S. El Din, Biodegradation of reactive black 5 by Aeromonas hydrophila strain isolated from dye-contaminated textile wastewater, Sustain. Environ. Res. 26 (5) (2016) 209–216.
[27] NorgenBiotek, Soil DNA isolation kit [cited 2021; Available from: https://norgenbiotek.com/sites/default/files/resources/Soil-DNA-Isolation-Plus-Kit-Insert-PI64000-1.pdf, 2016.
[28] F.T. Johra, et al., Facile and safe graphene preparation on solution based platform, J. Ind. Eng. Chem. 20 (5) (2014) 2883–2887.
[29] F.T. Thema, et al., Synthesis and characterization of graphene thin films by chemical reduction of exfoliated and intercalated graphite oxide, J. Chem. 2013 (2013), 150536.
[30] S.K. Bikkarolla, et al., Oxygen reduction reaction by electrochemically reduced graphene oxide, Faraday Discuss. 173 (2014) 415–428.
[31] A.M. Ruppert, et al., Synthesis of TiO2–ZrO2 mixed oxides via the alginate route: application in the ru catalytic hydrogenation of levulinic acid to gamma-valerolactone, Energies 12 (24) (2019).
[32] Q. Luo, et al., Preparation and characterization of ZrO2/TiO2 composite photocatalytic film by micro-arc oxidation, Trans. Nonferrous Metals Soc. China 23 (10) (2013) 2945–2950.
[33] G.G. Siu, et al., Variation of fundamental and higher-order raman spectra of ZrO2 nanograins with annealing temperature, Phys. Rev. B 59 (4) (1999) 3173–3179.
[34] M. Ocaña, et al., Low-temperature nucleation of rutile observed by raman spectroscopy during crystallization of TiO2, J. Am. Ceram. Soc. 75 (7) (1992) 2010–2012.
[35] S.K. Bikkarolla, et al., A three-dimensional Mn3O4 network supported on a nitrogenated graphene electrocatalyst for efficient oxygen reduction reaction in alkaline media, J. Mater. Chem. A 2 (35) (2014) 14493–14501.
[36] W. Zou, et al., Preparation of a graphene oxide membrane for air purification, Mater. Res. Express 6 (10) (2019), 105624.
[37] Y. Hu, et al., Zeolitic imidazolate Framework/Graphene oxide hybrid nanosheets as seeds for the growth of ultrathin molecular sieving membranes, Angew. Chem. Int. Ed. 55 (6) (2016) 2048–2052.
[38] L. Wang, et al., Significant catalytic effects induced by the electronic interactions between carboxyl and hydroxyl group modified carbon nanotube supports and vanadium species for NO reduction with NH3 at low temperature, Chem. Eng. J. 254 (2014) 399–409.
[39] Y.J. Oh, et al., Oxygen functional groups and electrochemical capacitive behavior of incompletely reduced graphene oxides as a thin-film electrode of supercapacitor, Electrochim. Acta 116 (2014) 118–128.
[40] O. Vieira, et al., Nitrogen-doped reduced graphene oxide – PVDF nanocomposite membrane for persulfate activation and degradation of water organic micropollutants, Chem. Eng. J. 402 (2020), 126117.
[41] A. Keck, et al., Reduction of azo dyes by redox mediators originating in the naphthalenesulfonic acid degradation pathway of sphingomonas sp. Strain BN6, Appl. Environ. Microbiol. 63 (9) (1997) 3684–3690.
[42] J. Wang, et al., Graphene oxide as an effective barrier on a porous nanofibrous membrane for water treatment, ACS Appl. Mater. Interfaces 8 (9) (2016) 6211–6218.
[43] R. Yi, et al., Selective reduction of epoxy groups in graphene oxide membrane for ultrahigh water permeation, Carbon 172 (2021) 228–235.
[44] K. Xu, et al., Synthesis of highly stable graphene oxide membranes on polydopamine functionalized supports for seawater desalination, Chem. Eng. Sci. 146 (2016) 159–165.
[45] Y. Han, et al., Ultrathin graphene nanofiltration membrane for water purification, Adv. Funct. Mater. 23 (29) (2013) 3693–3700.
[46] Y. Lou, et al., A facile way to prepare ceramic-supported graphene oxide composite membrane via silane-graft modification, Appl. Surf. Sci. 307 (2014) 631–637.
[47] L. Chen, et al., High performance graphene oxide nanofiltration membrane prepared by electrospraying for wastewater purification, Carbon 130 (2018) 487–494.
[48] S.-A. Ong, et al., Decolorization of azo dye (Orange II) in a sequential UASB–SBR system, Sep. Purif. Technol. 42 (3) (2005) 297–302.
[49] Y. García-Martínez, et al., Biodegradation of acid orange 7 in an anaerobic–aerobic sequential treatment system, Chem. Eng. Process. Process Intensif. 94 (2015) 99–104.
[50] G. Mezohegyi, et al., Effective anaerobic decolorization of azo dye acid Orange 7 in continuous upflow packed-bed reactor using biological activated carbon system, Ind. Eng. Chem. Res. 46 (21) (2007) 6788–6792.
[51] S.D. Ovhal, et al., Photocatalytic wet peroxide assisted degradation of Orange II dye by reduced graphene oxide and zeolites, J. Chem. Technol. Biotechnol. 96 (2) (2021) 349–359.
[52] S. Lee, et al., Well-wrapped reduced graphene oxide nanosheets on Nb3O7(OH) nanostructures as good electron collectors and transporters for efficient photocatalytic degradation of rhodamine B and phenol, RSC Adv. 6 (43) (2016) 37180–37188.
[53] X. Tan, D. Rodrigue, A review on porous polymeric membrane preparation. Part II: production techniques with polyethylene, polydimethylsiloxane, polypropylene, polyimide, and polytetrafluoroethylene, Polymers 11 (8) (2019).
[54] M. Rahimi, et al., Using Y-shaped microreactor for continuous decolorization of an azo dye, Desalin. Water Treat. 52 (28–30) (2014) 5513–5519.
[55] I. Meitiniarti, et al., Optimum concentration of glucose and Orange II for growth and decolorization of Orange II by enterococcus faecalis ID6017 under static culture, Microb. Indones. 2 (2008) 73–78.
[56] J. Ding, et al., Anaerobic biodecolorization of AO7 by a newly isolated Fe(III)-reducing bacterium sphingomonas strain DJ, J. Chem. Technol. Biotechnol. 90 (1) (2015) 158–165.
[57] X. Xiao, et al., A simple method for assaying anaerobic biodegradation of dyes, Bioresour. Technol. 251 (2018) 204–209.
[58] E. Franciscon, et al., Microaerophilic–aerobic sequential decolourization/biodegradation of textile azo dyes by a facultative klebsiella sp. Strain VN-31, Process Biochem. 44 (4) (2009) 446–452.
[59] A.Y.I. Ewida, et al., Complete degradation of azo dye acid red 337 by Bacillus megaterium KY848339.1 isolated from textile wastewater, Water Sci. 33 (1) (2019) 154–161.
[60] B.-Y. Chen, et al., Immobilized cell fixed-bed bioreactor for wastewater decolorization, Process Biochem. 40 (11) (2005) 3434–3440.
[61] S. Popli, U.D. Patel, Destruction of azo dyes by anaerobic–aerobic sequential biological treatment: a review, Int. J. Environ. Sci. Technol. 12 (1) (2015) 405–420.
[62] R. Khan, et al., Microbial decolorization and degradation of synthetic dyes: a review, Rev. Environ. Sci. Biotechnol. 12 (1) (2013) 75–97.
[63] C.-C. Hsueh, B.-Y. Chen, Comparative study on reaction selectivity of azo dye decolorization by Pseudomonas luteola, J. Hazard. Mater. 141 (3) (2007) 842–849.
[64] M. Solís, et al., Microbial decolouration of azo dyes: a review, Process Biochem. 47 (12) (2012) 1723–1748.
[65] B.-Y. Chen, Understanding decolorization characteristics of reactive azo dyes by Pseudomonas luteola: toxicity and kinetics, Process Biochem. 38 (3) (2002) 437–446.
[66] S. Garcia-Segura, et al., Comparative decolorization of monoazo, diazo and triazo dyes by electro-Fenton process, Electrochim. Acta 58 (2011) 303–311.
[67] Y.-N. Liu, et al., Exclusive extracellular bioreduction of methyl Orange by azo reductase-free geobacter sulfurreducens, Environ. Sci. Technol. 51 (15) (2017) 8616–8623.
[68] Z. Fang, et al., Performance of microbial fuel cell coupled constructed wetland system for decolorization of azo dye and bioelectricity generation, Bioresour. Technol. 144 (2013) 165–171.
[69] X. Cai, et al., Transcriptomic, proteomic, and bioelectrochemical characterization of an exoelectrogen geobacter soli grown with different electron acceptors, Front. Microbiol. 9 (2018) 1075.
[70] D. Sun, et al., Characterization of the genome from geobacter anodireducens, a strain with enhanced current production in bioelectrochemical systems, RSC Adv. 9 (44) (2019) 25890–25899.
[71] M.S. Khehra, et al., Comparative studies on potential of consortium and constituent pure bacterial isolates to decolorize azo dyes, Water Res. 39 (20) (2005) 5135–5141.
[72] G. Yang, et al., Pseudomonasguangdongensis sp. Nov., isolated from an electroactive biofilm, and emended description of the genus pseudomonas migula 1894, Int. J. Syst. Evol. Microbiol. 63 (Pt_12) (2013) 4599–4605.
[73] A.C. Jaramillo, et al., Degradation of adsorbed azo dye by solid-state fermentation: improvement of culture conditions, a kinetic study, and rotating drum bioreactor performance, Water Air Soil Pollut. 228 (6) (2017) 205.